

Mirror symmetry in magnetization reversal and coexistence of positive and negative exchange bias in Ni/FeF₂

M. Kovylna,^{1,a)} M. Erekhinsky,² R. Morales,³ I. K. Schuller,² A. Labarta,¹ and X. Batlle^{1,b)}

¹Fundamental Physics Departament and IN2UB, Universitat de Barcelona, 08028 Barcelona, Spain

²Department of Physics, University of California San Diego, La Jolla, 92093 California, USA

³University of the Basque Country and IKERBASQUE, 48011 Bilbao, Spain

(Received 27 January 2011; accepted 22 March 2011; published online 15 April 2011)

Positively and negatively exchange biased (PEB and NEB) magnetoresistance (MR) loops in Ni/FeF₂ ferromagnetic/antiferromagnetic (AF) heterostructures proceed through the same reversal mechanisms. The MR curves exhibit mirror symmetry: the increasing (decreasing) field branch of the PEB (NEB) loop is identical to the decreasing (increasing) branch of the NEB (PEB) loop, suggesting that the interfacial areal density of pinned uncompensated AF spins responsible for PEB and NEB is similar. Micromagnetic simulations are in agreement with experimental results and imply the coexistence of EB domains of opposite sign for all cooling fields, which results in a reversal mechanism not previously reported. © 2011 American Institute of Physics.

[doi:10.1063/1.3577648]

Exchange coupling across antiferromagnetic/ferromagnetic (AF/FM) interfaces leads to exchange bias (EB).¹ One of the salient manifestations of EB is the shift in the hysteresis loop (the EB field), either opposite or along the cooling field (H_{FC}), leading to negative¹ or positive² EB (NEB or PEB), respectively. The PEB is determined by the interplay between the AF coupling at the FM/AF interface and the Zeeman energy of pinned uncompensated interface and bulk AF spins.³ The transition from NEB to PEB is a function of H_{FC} and it can be either gradual² or discontinuous. The latter proceeds through a bi-domain state characterized by double hysteresis loops (DHLs) with coexistence of PEB and NEB regions at intermediate H_{FC} .⁴ These two distinct transitions depend on the relative sizes of the FM domains and the AF regions for which the pinned uncompensated interfacial AF spins induce the same unidirectional anisotropy in the FM.⁴ These regions are defined as the “EB domains.” When the transition from NEB to PEB is gradual (proceeds through the bidomain state), the EB domains are smaller (larger) than the FM ones. A number of questions are open concerning the origin of uncompensated spins and size of the EB domains,⁵ the role of interfacial and bulk AF spins,^{3,6,7} and the magnetization reversal mechanisms.⁸

In this letter, we investigate magnetization reversal in Ni/FeF₂. Magnetoresistance (MR) curves with negatively or positively shifted loops show striking mirror symmetry. This suggests that the interfacial areal density of pinned uncompensated AF spins responsible for NEB and PEB is similar thus producing the same reversal mechanisms. Micromagnetic simulations are in agreement with experimental results and imply the persistence of NEB (PEB) domains even at high (low) cooling fields, when MR curves show only PEB (NEB) loops.

Electron beam evaporation was used to fabricate Al(4 nm)/Ni(34 nm)/FeF₂(55 nm) heterostructures onto (110)MgF₂ single-crystal substrates.³ X-ray diffraction showed that FeF₂ grew epitaxial and untwinned in the (110)

orientation with the easy axis along [001] direction, which coincides with the growth-induced easy axis of the polycrystalline Ni layer.⁴ Photolithography and plasma etching were combined to obtain a series of heterostructures in the form of $90 \times 10 \mu\text{m}^2$ stripes.⁹ The long side of the stripes (x-axis) was patterned along the FeF₂[001] easy axis, determining the parallel direction for the injected dc current, H_{FC} and external field (H).⁹ A four-probe method was used to measure the MR curves (see Ref. 3 for details), at 4.2 K after field cooling the sample in H_{FC} from a saturated state at 150 K. The MR is defined as $\text{MR} = [R(H) - R_{\text{sat}}] / R_{\text{sat}}$, $R(H)$ and R_{sat} being the resistances at a field H and at the largest applied field, respectively (Fig. 1). The MR is normalized to the absolute value of the maximum MR for the decreasing field sweep (DS), MR_{DS} , i.e., $\text{MR}_{\text{norm}} = \text{MR} / \text{MR}_{\text{DS}}$ (Figs. 2 and 3).

The MR curves [inset to Fig. 1(a)] show negative (positive) shifts for H_{FC} below 0.6 kOe (above 4 kOe), while for intermediate H_{FC} , DHLs are observed. The strong similarity between the NEB and PEB peaks suggests the existence of mirror symmetry between the two cases. The PEB branch ($H_{FC} = 20$ kOe) for increasing field sweep (IS) collapses onto the NEB branch ($H_{FC} = 0.5$ kOe) for DS, provided that the latter is plotted as a function of $-H$ [Fig. 1(a)]. Figure 1(b) shows the same matching between the corresponding PEB DS branch and the NEB IS branch. This implies that the NEB and PEB loops proceed through exactly the same reversal mechanisms. We emphasize that this mirror symmetry has been observed in all (more than 20) investigated samples. These trends suggest that, similar average EB domain configurations of opposite sign are achieved for low and high H_{FC} .¹⁰

Figure 1(a) shows three distinct regions in the PEB MR loops: first, a gradual decrease (region I), followed by an abrupt jump down (region II), and finally a gradual increase (region III). Regions II and III have been associated with in-plane domain wall nucleation and propagation, followed by incoherent rotation of an in-volume incomplete domain wall within the FM.^{8,11,12} However, the reversal mechanism responsible for the field dependence in region I has not been identified yet. Although a single PEB peak is observed, the

^{a)}Electronic mail: miroslavna@ffn.ub.es.

^{b)}Electronic mail: xavierbatlle@ub.edu.

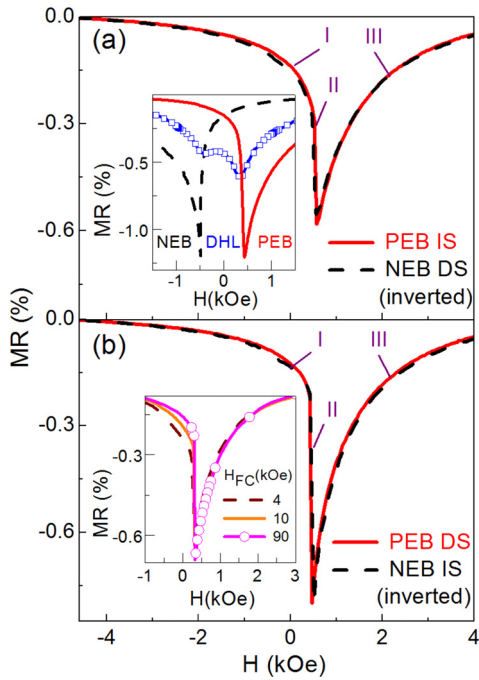


FIG. 1. (Color online) $MR = [R(H) - R_{sat}] / R_{sat}$ at 4.2 K, after cooling under $H_{FC} = 0.5$ kOe (dashed black line for NEB) and 20 kOe (solid red line for PEB): (a) IS for PEB and DS for NEB, the latter plotted as a function of $-H$ (inverted); (b) DS for PEB and IS for NEB, the latter plotted as a function of $-H$ (inverted). Inset to Fig. 1(a): MR curves for NEB (DHL; DS) and PEB (DS), respectively, for $H_{FC} = 0.5, 1,$ and 20 kOe. Inset to Fig. 1(b): MR in the PEB case (DSs) for $H_{FC} = 4, 10,$ and 90 kOe.

gradual increase in region I is progressively more abrupt as H_{FC} is increased from 4 to 90 kOe [inset Fig. 1(b)], which cannot be obtained assuming that for large H_{FC} , purely PEB domains exist and the pinned uncompensated interfacial AF spins are all frozen along the H_{FC} direction. This would produce an abrupt jump toward $MR = 0$ in region II, due to the complete Ni moment reversal produced by H , together with the AF coupling of the uncompensated pinned spins at the AF/FM interface. We define as “PEB (NEB) domains” the pinned uncompensated AF spins which form a domain and give rise to PEB (NEB). These experimental observations can be explained as due to the presence of minority EB do-

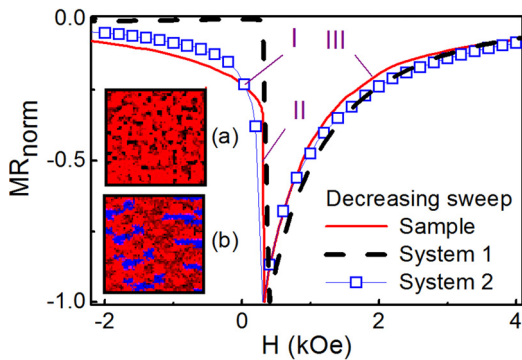


FIG. 2. (Color online) PEB case. Normalized MR, $MR_{norm} = MR / MR_{DS}$, with MR_{DS} being the absolute value of the maximum MR for DS, for $H_{FC} = 90$ kOe. DSs: experimental results (red solid line); micromagnetic simulations in the absence of NEB domains (black dashed line; System 1); and with the presence of a 20% of NEB domains (blue squares; System 2). The inset (a) [inset (b)] shows the spatially inhomogeneous effective field H_{eff} created by the uncompensated frozen AF spin distribution in the absence (presence) of NEB domains (System 1/System 2). The red regions in the inset (a) correspond to PEB domains; while the red (blue) regions in the inset (b) correspond to PEB (NEB) domains (along $\pm x$ -axis).

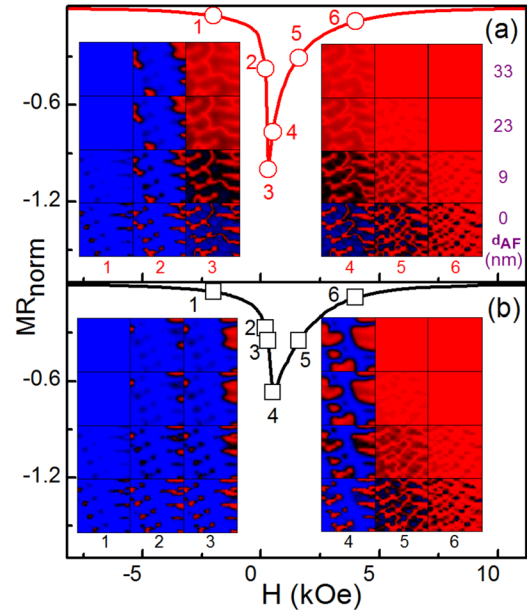


FIG. 3. (Color online) PEB case. Snap-shots of in-depth in-plane sections (top view) of the simulated FM film at 33, 23, 9, and 0 nm from the AF layer (d_{FM}) and at magnetic fields (kOe): $-2, 0.2, 0.3, 0.5, 1.6,$ and 4 , for both decreasing (a) and increasing (b) field sweeps. These magnetic fields correspond to labels 1, 2, 3, 4, 5, and 6, respectively, in the simulated MR curves. Red (blue) color corresponds to positive (negative) FM magnetization along x direction (M_x), while black color corresponds to $M_x = 0$.

mainly opposite in sign to H_{FC} . This implies the persistence, and gradual disappearance with increasing H_{FC} , of NEB domains even at high H_{FC} . The same features are also found for the decreasing branch of the PEB curve and for the NEB case in both field branches.

Magnetization reversal had already been studied by MR, in a Fe/MnF₂ sample grown on single crystal MgO, showing NEB.¹³ MnF₂ grows twinned, with a crystallographic coherence length of a few nanometers, in contrast to the untwinned single crystalline FeF₂ grown on (110)MgF₂, with much larger crystallographic coherence length (above 25 nm).^{4,5,10-12} As a result, the reversal mechanisms in the two cases are completely different. In twinned MnF₂/MgO,¹³ as H is reduced from positive saturation, coherent rotation is favored toward the easy axis at 45° from H . As H is increased from negative saturation, the unidirectional anisotropy leads to reverse domains. In untwinned FeF₂/MgF₂ (see Fig. 1 and inset for NEB), as H is reduced from positive saturation, the reversal starts at the FM/AF interface by the inversion of the Ni spins coupled to the minority PEB domains. This leads to an in-volume domain wall in region I. As H is increased from negative saturation, the unidirectional anisotropy favors reversal at the FM/AF interface by the inversion of the Ni spins coupled to the majority NEB domains, leading to an in-volume domain wall in region III [Fig. 2(a)].

The microscopic origin of region I was investigated by micromagnetic OOMMF (Ref. 14) simulations of a Ni film with area of 500×500 nm² and unit cell size of $5 \times 5 \times 2$ nm³. The energy terms for the calculations were: FM Zeeman coupling (E_{FMZ}), FM exchange (E_{EX}), FM anisotropy (E_A), and FM/AF interfacial coupling ($E_{FM/AF}$). The anisotropy of Ni film was modeled as a sum of: (i) randomly oriented Ni grains ($K_c = 5$ kJ/m³); (ii) in-plane shape anisotropy ($K_d = 150$ kJ/m³); and (iii) growth-induced uniaxial

anisotropy along the x axis ($K_u=20$ kJ/m³). The frozen AF moments¹² were assumed to produce a surface monolayer of spatially inhomogeneous, pinned uncompensated moments, with overall spin coverage of 7%.¹⁵ These are coupled to the bottom FM layer, creating an effective magnetic field, H_{eff} . AF grains with average area of about 25×25 nm², with an angular distribution of the AF easy axes, and an inhomogeneous interfacial coupling were introduced in the simulation (see Ref. 12 for details).

The anisotropic MR arises only from FM Ni, since FeF₂ is an insulator. Therefore, the local magnetization configurations obtained from the simulations were used to calculate the MR(H) in the parallel current-to-field geometry, which is proportional to the sum of the square of the transverse component of the local magnetization.

A variety of situations were studied: (i) inhomogeneous interfacial AF/FM coupling; (ii) different ratios between the AF/FM coupling and induced FM anisotropy; (iii) variations in the FM layer thickness; (iv) FM and AF easy axis distribution. Although all these factors captured the features in regions II and III, none of them, neither their combinations, produced a gradual MR saturation in region I. Only the introduction of EB domains of opposite sign enabled the simulations to capture the experimental features of region I.

Figure 2 compares the experimental MR of a PEB sample with the simulation for two systems. In one, only EB domains which may induce PEB are present, while, in the other, a minority of EB domains inducing NEB is present. The system without NEB domains [H_{eff} is shown in the inset (a) to Fig. 2] is in agreement with experimental MR data in regions II and III, but fails to reproduce the gradual saturation in region I. When $\sim 20\%$ NEB domains are included [H_{eff} is shown in the inset (b) to Fig. 2], the simulation is in very good agreement with experimental MR loops. The same agreement with the experimental results is obtained for the NEB case with $\sim 20\%$ of PEB domains. The persistence of NEB (PEB) domains even at high (low) cooling fields may be produced by the size distribution and density of pinned uncompensated moments in the bulk of the AF.^{3,6,10} In the AF, both the pinned uncompensated interface spins (responsible for the loop shift) and bulk spins (responsible for the onset of PEB and relative ratio of PEB to NEB for a given H_{FC}) align with the cooling field. This is because they belong to the same domain and become pinned below T_N , in agreement with the domain state model.⁷

The micromagnetic configurations corresponding to PEB are shown in Fig. 3 for the H_{eff} displayed in the inset (b) to Fig. 2. In positive saturation for the decreasing field branch [Fig. 3(a)], the FM is uniformly saturated. For PEB domains, the FM exchange and FM Zeeman coupling ($E_{\text{EX}}+E_{\text{FMZ}}$) dominate over the AF coupling at the FM/AF interface ($E_{\text{FM/AF}}$), favoring alignment of the FM layer with H . For NEB domains, those three energy terms also stabilize FM in the field direction. With decreasing field toward 6, $|E_{\text{FMZ}}+E_{\text{EX}}|$ becomes smaller than $|E_{\text{FM/AF}}|$ for the Ni spins in contact with PEB domains, giving rise to local magnetization reversal. Following this nucleation at the bottom of the FM, propagation of inverted domains takes place as H is further decreased from 5 to 3, evolving both upwards through the

depth of the FM and laterally (in-volume domain wall in region III). As 3 is approached, the slope of MR steadily increases until the maximum misalignment between FM spins and current direction is reached, which corresponds to the MR minimum. As this minimum is crossed, the top FM layer abruptly reverses [label 2 in Fig. 3(a)] by lateral in-plane domain wall nucleation and propagation (region II). However, the reversal of the top FM layer in the negative direction creates in-depth structures over the minority NEB domains because the Ni spins close to the interface are still pinned in positive direction by the interfacial AF coupling (region I). As H is further decreased [label 1 in Fig. 3(a)], the in-depth structures associated with the residual NEB domains shrink in all directions, as all the FM spins are aligned along the negative field direction. With IS [Fig. 3(b)], the reversal sequence is inverted. The same in-depth structures take place in the NEB case in both field branches.

In summary, PEB and NEB loops in Ni/FeF₂ exhibit the same reversal mechanisms, showing perfect mirror symmetry between decreasing and increasing field branches. The latter suggests that, on average, similar but opposite sign EB domain configurations are reached for low or high cooling fields, with equal interfacial density of pinned uncompensated AF spins responsible for NEB or PEB. Micromagnetic simulations are in agreement with the experimental results and imply the persistence of NEB (PEB) domains even at the highest (lowest) cooling fields.

The authors are indebted to Dr. Zhi-Pan Li and Prof. M. Kiwi for comments on the manuscript. The support of the Spanish MICINN (Grant Nos. MAT2009-08667, FIS2008-06249, FICYTIB08-106) and Catalan DURSI (Grant No. 2009SGR856), U. Barcelona, IKERBASQUE, and the U.S. Department of Energy are recognized.

¹J. Nogués and I. K. Schuller, *J. Magn. Magn. Mater.* **192**, 203 (1999).

²J. Nogués, D. Lederman, T. J. Moran, and I. K. Schuller, *Phys. Rev. Lett.* **76**, 4624 (1996).

³M. Kovylyna, M. Erekhinsky, R. Morales, J. Villegas, I. K. Schuller, A. Labarta, and X. Batlle, *Appl. Phys. Lett.* **95**, 152507 (2009).

⁴I. V. Roshchin, O. Petravic, R. Morales, Z.-P. Li, X. Batlle, and I. K. Schuller, *Europhys. Lett.* **71**, 297 (2005).

⁵O. Petravic, Z.-P. Li, I. V. Roshchin, M. Viret, R. Morales, X. Batlle, and I. K. Schuller, *Appl. Phys. Lett.* **87**, 222509 (2005).

⁶R. Morales, Z.-P. Li, J. Olamit, K. Liu, J. M. Alameda, and I. K. Schuller, *Phys. Rev. Lett.* **102**, 097201 (2009).

⁷P. Miltényi, M. Gierlings, J. Keller, B. Beschoten, G. Güntherodt, U. Nowak, and K. D. Usadel, *Phys. Rev. Lett.* **84**, 4224 (2000).

⁸R. Morales, M. Vélez, O. Petravic, I. V. Roshchin, Z.-P. Li, X. Batlle, J. M. Alameda, and I. K. Schuller, *Appl. Phys. Lett.* **95**, 092503 (2009).

⁹M. Kovylyna, M. Erekhinsky, R. Morales, I. K. Schuller, A. Labarta, and X. Batlle, *Nanotechnology* **21**, 175301 (2010).

¹⁰M. R. Fitzsimmons, B. J. Kirby, S. Roy, Z.-P. Li, I. V. Roshchin, S. K. Sinha, and I. K. Schuller, *Phys. Rev. B* **75**, 214412 (2007).

¹¹R. Morales, Z.-P. Li, O. Petravic, X. Batlle, and I. K. Schuller, *Appl. Phys. Lett.* **89**, 072504 (2006).

¹²Z.-P. Li, O. Petravic, R. Morales, J. Olamit, X. Batlle, K. Liu, and I. K. Schuller, *Phys. Rev. Lett.* **96**, 217205 (2006).

¹³I. N. Krivorotov, C. Leighton, J. Nogués, I. K. Schuller, and E. D. Dahlberg, *Phys. Rev. B* **65**, 100402(R) (2002).

¹⁴See <http://math.nist.gov/oommf/> for details.

¹⁵P. Kappenberger, S. Martin, Y. Pellmont, H. J. Hug, J. B. Kortright, O. Hellwig, and E. E. Fullerton, *Phys. Rev. Lett.* **91**, 267202 (2003).